IUST Iran University of Science and Technology

Iranian Journal of Electrical and Electronic Engineering

Journal Homepage: ijeee.iust.ac.ir

Research Paper

# Singular Perturbation Theory for PWM AC/DC Converters: Cascade Nonlinear Control Design and Stability Analysis

Y. Mchaouar*(C.A.), A. Abouloifa*, I. Lachkar**, H. Katir*, F. Giri***, A. El Aroudi****, A. Elallali*, and C. Taghzaoui*

**Abstract:** In this paper, the problem of controlling PWM single-phase AC/DC converters is addressed. The control objectives are twofold: (i) regulating the output voltage to a selected reference value, and (ii) ensuring a unitary power factor by forcing the grid current to be in phase with the grid voltage. To achieve these objectives, the singular perturbation technique is used to prove that the power factor correction can be done in the open-loop system with respect to certain conditions that are not likely to take place in reality. It is also applied to fulfill the control objectives in the closed-loop through a cascade nonlinear controller based on the three-time scale singular perturbation theory. Additionally, this study develops a rigorous and complete formal stability analysis, based on multi-time-scale singular perturbation and averaging theory, to examine the performance of the proposed controller. The theoretical results have been validated by numerical simulation in MATLAB/Simulink/SimPowerSystems environment.

**Keywords:** Singular Perturbation, PWM AC/DC Converters, Nonlinear Control, Power Factor Correction, Averaging Theory, Stability Analysis.

## 1 Introduction

WITH the emergence of DC power sources in various industrial applications [1] (such as plug-in and hybrid electric vehicles, DC-motor drives, personal computers, telecommunications, household-electric appliances, etc.), AC/DC power conversion systems are widely used to connect AC sources with DC loads. From a control point of view, these converters have their drawbacks that reside basically in the complexity of their models (non-linear, non-minimal phase, hybrid system), which often results the generation of undesirable current harmonics when the converter is connected to an AC power source contributing to the disturbance of the electrical grid. To avoid these drawbacks, converter controllers should not only aim at regulating the output voltage but also at power factor correction (PFC). The last objective is to eliminate all undesirable current harmonics when the converter is connected to the power supply.

Recently, two main goals have been taken considered simultaneously in the control design for AC/DC converters: power factor correction and DC output voltage regulation.

In this respect, several control methods have been proposed. In [2] and [3], authors have proposed control strategies involving a single-loop controller based on the passivity technique and the bidirectional current sensorless control (BCSC), but these solutions are only applicable for constant loads and reference voltages. In [4] and [5], the singular perturbation was applied to design continuous and digital controllers, but no

Iranian Journal of Electrical and Electronic Engineering, 2022.
Paper first received 16 October 2020, revised 07 May 2021, and accepted 28 May 2021.
* The authors are with the TI Lab., Faculty of Sciences Ben M'sik, Hassan II University of Casablanca, Casablanca, Morocco.
E-mails: uns1mchaouar@gmail.com, a.abouloifa@gmail.com, katir.hanane@gmail.com, aichaelallali@gmail.com, and taghzaouichaimaa@gmail.com.
** The author is with the ESE Laboratory, ENSEM, Hassan II University of Casablanca, Casablanca, Morocco.
E-mail: lachkaribtissam@gmail.com.
*** The author is with the Automatic Laboratory of Caen (LAC), National Graduate School of Engineering of Caen (ENSICAEN), University of Caen Normandy, Caen, France.
E-mail: fouad.giri@unicaen.fr.
**** The author is with the Department of Electronic, Electrical and Automatic Engineering, University of Rovira i Virgili (URV), Tarragona, Spain.
E-mail: abdelali.elaroudi@urv.cat.
Corresponding Author: Y. Mchaouar.
https://doi.org/10.22068/IJEEE.18.1.2013

rigorous analysis was performed to prove that the proposed controllers could achieve the desired performance. Other approaches were suggested including sliding mode [6], backstepping technique [7], and Feedback linearization control [8]. However, most of these researches do not include a study of the open-loop system. In addition, the proposed studies have been built on the assumption that resistance losses are negligible as discussed in [9]. As result, by the present study, we are suggesting a more rigorous analysis of the open-loop dynamics of the rectifier establishing how the power factor correction can be best assured related to the inductance, capacitance, load, and parasitic resistances. For the control system, a high-gain output feedback controller [10, 11] is designed using the singular perturbation approach [12, 13], where the three-time scale separation process is induced in the closed-loop system with two cascaded loops: (i) the inner loop is required to ensure that the converter's input current is sinusoidal and in phase with the supply voltage of the grid, and (ii) The outer loop is built to regulate the output voltage by tuning the inner loop reference. The theoretical analysis of the stability of the resulting closed-loop system is one of the major motivations of the present work, It is based on the averaging theory (Chapter 10 in [12]) [7, 14] and the three-timescale singular perturbation (Chapter 11 in [12]) and [15].

The contribution of the present study is different from previous work in many aspects, including the following:

1. This is the first time that a rigorous and complete analysis of the dynamics of the open-loop AC/DC converters has been carried out to examine the power factor correction. Previous researches missed an open-loop formal study [2], [3], [6], [7]. For this purpose, a relationship among inductance, capacitance, and parasitic resistances (which were ignored in most previous studies [6], [7], [9]) is established using the singular perturbation technique.
2. It is formally proven in this study that the control objectives (i.e. Power Factor Correction and DC voltage regulation) are successfully accomplished by a systematic theoretical analysis focusing, for the first time, on new techniques such as three-time scale singular perturbation and averaging theory. Previous researches lacked a closed-loop formal analysis [2-5], [8].

The paper is structured as follows: Section 2 starts with the averaged and normalized model. Next, the singular perturbation technique is adopted to the normalized average model in order to establish an algebraic relationship between the fast variable "inductor current" and the slow variable "capacitor voltage" via an integral manifold. The system is modified in Section 3 by a non-linear controller containing two cascaded loops. Section 4 addresses the stability of a three-time-scale closed-loop system. Finally, numerical simulations in Section 5 demonstrate the performance of the controller, followed by a conclusion and a list of the consulted reference.

## 2 Open Loop

### 2.1 Instantaneous Model

The PWM boost rectifier, shown in Fig. 1, is mainly composed of a full-bridge based on two switching cells called ($S_1$, $S_3$) and ($S_2$, $S_4$). It connects the supply network, which behaves with the inductance $L$ in series as a current source, to the assembly ($R$, $C$) whose nature is of the voltage source type. This power converter is driven by a binary signal $\mu = \{-1, 1\}$ produced by a PWM generator.

The dynamic behavior of the Full-bridge PWM rectifier is expressed by the instantaneous model, which is directly derived from Kirchhoff's laws. This mathematical model describes the operation of the circuit in continuous conduction mode.

$$\frac{di_n}{dt} = -\frac{r_L}{L} i_n - \frac{\mu}{L} v_o + \frac{v_n}{L} \tag{1a}$$

$$\frac{dv_o}{dt} = \frac{\mu}{C} i_n - \frac{v_o}{RC} \tag{1b}$$

From a modeling point of view, the current $i_n$ and the voltage $v_o$ represent the state variables of the target system. The grid voltage $v_n$ is given by:

$$v_n = E_n \sin(\omega_n t) \tag{2}$$

### 2.2 Averaging Model

Due to the discontinuous nature of the switched model, (1a) and (1b) the behavior system analysis is relatively complicated. One well-known modeling approach of such systems relies on approximating their operation by "averaging techniques" [16-18]. By applying the KBM technique developed up to the first order only [17], the state-space-averaged system of (1a) and (1b) becomes:

$$\frac{dx_1}{dt} = -\frac{r_L}{L} x_1 - \frac{u}{L} x_2 + \frac{v_n}{L} \tag{3a}$$

$$\frac{dx_2}{dt} = \frac{u}{C} x_1 - \frac{x_2}{RC} \tag{3b}$$

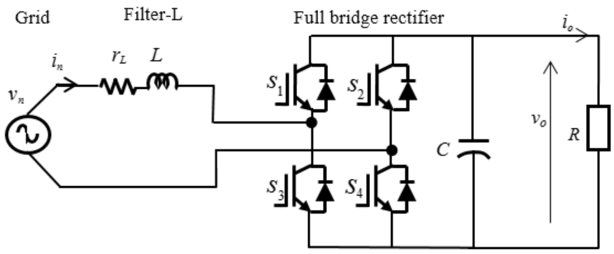


**Fig. 1** Full-bridge PWM boost rectifier.

where $x_1$, $x_2$, and $u$ denote the average values, over cutting periods $T_s$, of the signals $i_n$, $v_o$, and $\mu$. It should be noted that the selected average model conserves the non-linear character of the initial scheme. However, it does not take into account the ripples resulting from the switching of power semiconductors.

### 2.3 Normalized Model

This subsection is dedicated to normalizing the model in the appropriate form of a singularly perturbation system. For this purpose, voltages, currents, impedances, and time are respectively reduced with respect to the nominal output voltage $V_{On}$, the nominal output current $I_{On} = V_{On}/R$, the nominal load $R$, and the time constant $RC$. Table 1 gives the expressions of the main reduced quantities.

The normalized model is then stated as follows:

$$\varepsilon_0 \frac{dx_f}{dt_n} = f_f(x_s, x_f, u, w) \tag{4a}$$

$$\frac{dx_s}{dt_n} = f_s(x_s, x_f, u, w) \tag{4b}$$

where $f_f(x_s, x_f, u, w) = -\sigma x_f - u x_s + w$ and $f_s(x_s, x_f, u, w) = u x_f - x_s$. $x_f$ and $x_s$ are the normalized state variables representing the fast mode and the slow mode respectively. $w$ is perceived as a disturbing input and the small positive parameter $\varepsilon_0$ indicates the speed ratio between slow and fast phenomena in the system.

### 1.1 Open-loop analysis via singular perturbation

The normalized model is examined to find a definitive relationship that specifies whether (or not) the time-scales separation criteria [19] is achieved in the present system. Therefore, the two-time-scale singular perturbation technique is applied to the system (4a) and (4b) ([12, 13]). In fact, in steady-state, the integral manifold, which is given by Taylor series development in (5), characterizes the behavior of the fast variable $x_f$.

$$\begin{aligned}\lim_{t_n\to\infty} x_f &= \Phi_\varepsilon(x_s, u, w) \\ &= \varphi_0(x_s, u, w) + \varepsilon_0\varphi_1(x_s, u, w) + O(\varepsilon_0^2)\end{aligned} \tag{5}$$

The $O(\varepsilon_0^2)$ terms can often be neglected. The retention of $\varphi_1$ improves precision for moderate values of $\varepsilon_0$.

During the transitional regime, $x_f$ cannot be on the integral manifold. Therefore, the deviation between the state and its value for the quasi-stationary situation is as follows:

**Table 1** The normalized state variables and parameters.

| Normalized quantities | Values |
|---|---|
| $x_f$ | $x_1R/V_{On}$ |
| $x_s$ | $x_2/V_{On}$ |
| $w$ | $v_n/V_{On}$ |
| $\sigma$ | $r_L/R$ |
| $t_n$ | $t/RC$ |
| $T_{sn}$ | $T_s/RC$ |
| $\varepsilon_0$ | $L/R^2C$ |

$$\Gamma = x_f - \Phi_\varepsilon(x_s, u, w) \tag{6a}$$

According to (5) and (6a), one gets:

$$x_f \approx \varphi_0(x_s, u, w) + \varepsilon_0\varphi_1(x_s, u, w) + \Gamma \tag{6b}$$

The time derivative of $x_f$ evaluated along the manifold $\Phi_\varepsilon$ can be written as:

$$\varepsilon_0 \frac{dx_f}{dt_n} = \varepsilon_0 \frac{d\Phi_\varepsilon}{dt_n} = \varepsilon_0 \frac{\partial \Phi_\varepsilon}{\partial x_s}\frac{dx_s}{dt_n} \tag{7}$$

Taking into consideration (4a), (4b), and (7), the integral manifold condition is defined as follows:

$$\varepsilon_0 \frac{\partial \Phi_\varepsilon}{\partial x_s} f_s(x_s, \Phi_\varepsilon, u, w) = f_f(x_s, \Phi_\varepsilon, u, w) \tag{8}$$

In order to define asymptotic power series solutions of (5), we must also apply the Taylor series expansion for $f_f(x_s, \Phi_\varepsilon, u, w)$ and $f_s(x_s, \Phi_\varepsilon, u, w)$ to the region of $x_f = \varphi_0$. The most important of both series is:

$$\begin{aligned}f_f(x_s, \Phi_\varepsilon, u, w) &= f_f(x_s, \varphi_0, u, w) \\ &\quad + \frac{\partial f_f}{\partial x_f}(x_s, \varphi_0, u, w)\left(\Phi_\varepsilon - \varphi_0\right) \\ &\quad + \frac{1}{2}\frac{\partial^2 f_f(x_s, \varphi_0, u, w)}{\partial x_f^2}\left(\Phi_\varepsilon - \varphi_0\right)^2 \\ &\quad + \cdots\end{aligned} \tag{9}$$

Taking into account (5), Eq. (9) becomes:

$$\begin{aligned}f_f(x_s, \Phi_\varepsilon, u, w) &= f_f(x_s, \varphi_0, u, w) \\ &\quad + \frac{\partial f_f}{\partial x_f}(x_s, \varphi_0, u, w)\left(\varepsilon_0\varphi_1\right) \\ &\quad + \frac{1}{2}\frac{\partial^2 f_f(x_s, \varphi_0, u, w)}{\partial x_f^2}\left(\varepsilon_0\varphi_1\right)^2 + \cdots\end{aligned} \tag{10}$$

By substituting these expansions into the manifold condition given by (8) and equating terms in like powers of $\varepsilon_0$, it will take two steps to obtain $\varphi_0$ and $\varphi_1$

$$\varepsilon_0^{\,0}: \qquad 0 = f_f(x_s, \varphi_0, u, w) \tag{11a}$$

$$\varepsilon_0^{\,1}: \qquad \frac{\partial \varphi_0}{\partial x_s} f_s(x_s, \varphi_0, u, w) = \frac{\partial f_f}{\partial x_f}\varphi_1 \tag{11b}$$

In accordance with (4a) and (5), the dynamic behavior of $x_f$ can be reformulated in the following form:

$$\varepsilon_0 \frac{d}{dt_n}(\varphi_0 + \varepsilon_0\varphi_1 + \Gamma) = f_f(x_s, \varphi_0 + \varepsilon_0\varphi_1 + \Gamma, u, w) \tag{12}$$

The fact that $\varphi_0$ and $\varphi_1$ are known from (11a) and (11b) suggests that Eq. (12) can be reduced, where the time derivative of $\varphi_0$ and $\varphi_1$ are given by the next chain rule

$$\frac{d}{dt_n}(\varphi_0+\varepsilon_0\varphi_1)=(\frac{\partial\varphi_0}{\partial x_s}+\varepsilon_0\frac{\partial\varphi_1}{\partial x_s})f_S(x_s,\varphi_0+\varepsilon_0\varphi_1+\Gamma,u,w) \quad (13)$$

By solving (12), it is possible to find a useful form of Γ based on the form and details of the system. A critical requirement is that (12) must be stable, i.e. the off-manifold dynamics Γ must decay so that the state vector will converge to the manifold. According to the previous discussion and the solutions of Eq. (11a) and (11b), the expressions of $\varphi_0$ and $\varphi_1$ for the system (4a) and (4b) are given by:

$$\varphi_0=\frac{w-ux_s}{\sigma} \quad (14a)$$

$$\varphi_1=\frac{u^2w-u^3x_s-u\sigma x_s}{\sigma^3} \quad (14b)$$

Therefore, the off-manifold dynamics can be deduced from (12), (13), and (14), which can be simplified significantly to:

$$\varepsilon_0\frac{d\Gamma}{dt_n}=\left(\frac{\varepsilon_0u^2}{\sigma}-\sigma\right)\Gamma \quad (15)$$

The critical point in the applicability of the singular perturbation design methodology is that the fast dynamics must be decayed rapidly. Thus, $x_f$ will generally be on or near the integral manifold after fast transient damping and can be treated as algebraic rather than dynamic. In other words, this requires that the error term Γ has a stable equilibrium near the origin. To achieve this, the following algebraic condition must be fulfilled:

$$\frac{\varepsilon_0u^2}{\sigma}<<\sigma \quad (16)$$

As the above condition contains the exogenous input $u\in[-1, 1]$ and in order to make it as a generally applicable requirement, (16) may be expressed as follows:

$$\sqrt{\frac{L}{C}}<<r_L \quad (17)$$

Inequality (17) plays the role of timescale separation requirement corresponding to the open-loop full-bridge AC/DC rectifier.

**Remark 1.** In the present study, we have neglected the equivalent series resistance of the capacitor (ESR) named $r_C$ because of its small value compared to the other resistances. In the case where $r_C$ has a large value, we proceed with the same steps mentioned above. An expression similar to (17) given by an augmented requirement is found as: $\sqrt{\frac{L}{C}}<<(r_L+r_C)$.

## 3 Closed Loop System

### 3.1 Control Objectives

After performing an analysis of the open-loop system for the time-scale separation requirement, a non-linear controller is designed, based on the average model (3a) and (3b), to accomplish two main purposes:

1. PFC requirement: entails ensuring that, in steady-state, the input currents $i_n$ should be sinusoidal and in phase with the AC-line voltage source $v_n$.
2. Output voltage regulation: the DC component of the voltage $v_o$ should be driven to a given reference value $x_2^*$ keeping the elevating nature of the power converter under study.

To meet these requirements, a high gain non-linear output feedback controller [10] is developed using the singular perturbation approach [12, 13].

### 3.2 Power Factor Correction

#### 3.2.1 Controller Design

According to the PFC goal, the network current must follow a sinusoidal reference signal $x_2^*=\beta\sin(\omega_n t)$ of the same frequency and phase as the grid voltage $v_n$. At this point, $\beta$ is a real-time function that should converge, in steady-state, to a positive constant.

Let us begin with the current tracking error:

$$e_1=x_1^*-x_1 \quad (18a)$$

It is obvious from (3a) that the first derivative of $x_1(t)$ depends directly on the control input variable $u$. Hence, we will construct the reference model for (3a) in the form of the desired first-order stable ordinary differential equation:

$$\dot{x}_1=\frac{e_1}{T_1}+\dot{x}_1^*\overset{\text{def}}{=}D_1(x_1^*,x_1) \quad (18b)$$

where $T_1$ is the time constant of the desired dynamic for the current $x_1$. Based on (18b), the realization error of the desired behavior of $\dot{x}_1$, namely $\Omega_1$, is defined by:

$$\Omega_1=D_1(x_1^*,x_1)-\dot{x}_1 \quad (19)$$

Therefore, the control problem $\lim_{t\to\infty}e_1(t)=0$ relies on the insensitivity condition

$$\Omega_1=0 \quad (20)$$

Doing so, the behavior of $\dot{x}_1$ with the recommended dynamics of (18b) will be considered. Replacing $\dot{x}_1$ in the requirement (19) by its expression, (3a) yields to the following equation:

$$D_1(x_1^*, x_1) + \frac{r_L}{L}x_1 + \frac{u}{L}x_2 - \frac{v_n}{L} = 0 \tag{21}$$

The solution of (21) can be determined by several control laws, for example, the non-linear inverse dynamic control [20] is based on the analytical solution of (21) as given by

$$u_{id} = -\frac{L}{x_2}\left(D_1(x_1^*, x_1) + \frac{r_L}{L}x_1 - \frac{v_n}{L}\right) \tag{22}$$

According to (22), the nonlinear inverse dynamic solution requires precise information about the plant model parameters and external disturbances. This problem can be solved by applying a robust control law based on the application of higher-order output derivative jointly with a high gain in the controller so that the system is made exponentially stable. For this purpose, let us use the following Lyapunov candidate function:

$$V_1(u) = \frac{1}{2}\Omega_1^2(u) \tag{23a}$$

Using (19) and (21), the derivation function of the chosen Lyapunov candidate can be expressed as

$$\frac{dV_1(u)}{dt} = \frac{x_2}{L}\Omega_1\frac{du}{dt} \tag{23b}$$

Taking into account the fact that $x_2 > 0$, the system (3a) will be stable if the control law $u$ was chosen such that:

$$\frac{du}{dt} = \frac{k_1}{\varepsilon_1\varepsilon_2}\Omega_1 \tag{24}$$

where $\varepsilon_1$ and $\varepsilon_2$ are sufficiently small positive quantities and $k_1$ is a negative real-type design parameter.

As a result of (3a), (18), and (19), the high-gain control law takes the following dynamical expression

$$\varepsilon_1\varepsilon_2\frac{du}{dt} = k_1\left(\frac{e_1}{T_1} + \frac{u}{L}x_2 + \frac{r_L}{L}x_1 - \frac{v_n}{L} + \dot{x}_1^*\right) \tag{25}$$

**Remark 2.** The inverse $1/\varepsilon_1\varepsilon_2$ represents the high gain parameter due to $\varepsilon_1\varepsilon_2$ having a sufficiently small value. This implies that despite the bounded parameter variations and the presence of external disturbances, the desired dynamic properties of $x_1$ are provided in a specific region of the state space of the uncertain nonlinear system (3a).

### 3.2.2 Inner Loop Singular Perturbation System

The inner current loop, consisting of (3a) and (3b) and the non-linear control law (25), undergoes the following equations

$$\varepsilon_1\varepsilon_2\frac{dZ}{dt} = h_{UF}(X, Z, t) \tag{26a}$$

$$\frac{dX}{dt} = f_{Sinn}(X, Z, t) \tag{26b}$$

where: $Z = u$, $X = (x_1 \quad x_2)^T$, $h_{UF}(X, Z, t) = k_1\left[\frac{x_2 Z}{L} + \left(\frac{r_L}{L} - \frac{1}{T_1}\right)x_1 + \frac{x_1^*}{T_1} + \dot{x}_1^* - \frac{v_n}{L}\right]$, and $f_{Sinn}(X, Z, t) = \begin{pmatrix} -r_L x_1/L - x_2 Z/L + v_n/L \\ x_1 Z/C - x_2/RC \end{pmatrix}$.

For $\varepsilon_1$ sufficiently small, the above equations take the form of singularly perturbed differential equations. Passing to the ultra-fast time-scale $\tau_1 = t/\varepsilon_1\varepsilon_2$ and setting $\varepsilon_1 = 0$, the ultra-fast dynamic subsystem (UFDS) is defined by:

$$\frac{dZ}{d\tau_1} = h_{UF}(X, Z, t) \tag{27a}$$

$$\frac{dX}{d\tau_1} = 0 \tag{27a}$$

**Remark 3.** The variables $X$ and $\dot{x}_1^*$ are considered as the frozen parameters during the ultra-rapid transient in (27a).

Following the fast decay of the transients in (27a), the steady-state (more precisely, the quasi-steady-state) of the UFDS tends toward an equilibrium given by

$$Z^s = \left(\frac{L}{T_1} - r_L\right)\frac{x_1}{x_2} - \frac{L}{T_1 x_2}x_1^* - \frac{L}{x_2}\dot{x}_1^* + \frac{v_n}{x_2} \tag{28}$$

On the slow manifold, the slow dynamic subsystem (SDS) of the inner loop takes place by replacing the expression of $Z^s$ in (26b) by (28), one gets

$$\dot{X} = \begin{pmatrix} \frac{e_1}{T_1} + \dot{x}_1^* \\ -\frac{x_2}{RC} + \left(\frac{L}{CT_1} - \frac{r_L}{C}\right)\frac{x_1^2}{x_2} - \frac{L x_1 x_1^*}{CT_1 x_2} - \frac{L x_1 \dot{x}_1^*}{Cx_2} + \frac{v_n x_1}{Cx_2} \end{pmatrix} \tag{29}$$

The stability results are summed up in the proposition below.

**Proposition 1.** Consider the singular perturbation system of the inner loop composed of (26a) and (26b). According to Remark 3, one has the following properties:

1. If the gain $k_1$ is negative, the UFDS (27a) is exponentially stable and $Z$ converges exponentially fast to $Z^s$.
2. The behavior of $x_1$ is prescribed by a stable reference equation of the form $dx_1/dt = \dot{x}_1^* + e_1/T_1$. Following that, the requirement $\lim_{t\to\infty} e_1(t) = 0$ is

maintained.

3. If, in addition $\beta$ converges (to a positive limit value), then the PFC requirement is fulfilled.

### 3.3 Output Voltage Regulation

The second stage is to complete the inner control loop with an outer control loop. The objective is to design a tuning law for the ratio $\beta$ to control the output voltage $x_2$ to a selected reference value $x_2^*$.

#### 3.3.1 Controller Design

Based on the three-time scale singular perturbation technique, the fast inner current loop should be coupled with a slow outer voltage loop. In order to guarantee the time-scale separation between these two loops, the design parameters of the voltage loop, namely $\varepsilon_2$ and $T_2$ (which are designed later), must therefore meet the following requirements: $0 < \varepsilon_1\varepsilon_2 \ll \varepsilon_2 \ll 1$ and $T_1 < T_2$.

Firstly, it is necessary to identify the relationship between the DC output voltage $x_2$ (which represents the output signal of the outer loop), and the ratio $\beta$ (which acts as the control input).

This is established in the proposition that follows.

**Proposition 2.** Taking into account the resulting equation defined by (29) with the PFC requirement (where $x_1^* = \beta\sin(\omega_n t)$), the voltage $x_2$ varies according to the following first-order time-varying nonlinear equation in response to the tuning ratio $\beta$:

$$\frac{dx_2}{dt} = -\frac{x_2}{RC} + \frac{E_n\beta - r_L\beta^2 - L\dot{\beta}\beta}{2Cx_2} - \frac{\left(E_n\beta - r_L\beta^2 - L\dot{\beta}\beta\right)\cos(2\omega_n t) + L\beta^2\omega_n\sin(2\omega_n t)}{2Cx_2} \tag{30}$$

To synthesize the control law of the outer voltage loop, let us construct the desired behavior of $x_2$ in the following form:

$$\dot{x}_2 = (\dot{x}_2^* + \frac{e_2}{T_2}) \overset{\text{def}}{=} D_2(x_2^*, x_2) \tag{31}$$

where $e_2$ represents the voltage tracking error defined as

$$e_2 = x_2^* - x_2 \tag{32}$$

In the same way, as for the current loop, let us define the following desired dynamic realization error

$$\Omega_2 = D_2(x_2^*, x_2) - \dot{x}_2 \tag{33a}$$

and the insensitivity condition:

$$\Omega_2 = 0 \tag{33b}$$

To regulate the output voltage $x_2$ of the power converter to its reference value $x_2^*$; i.e., that is any positive constant satisfying $x_2^* > E_n$, the following dynamic control law is suggested [10]:

$$\varepsilon_2^2\frac{d^2\beta}{dt^2} + a\varepsilon_2\frac{d\beta}{dt} = k_2\left(\frac{e_2}{T_2} - \frac{de_2}{dt}\right) \tag{34}$$

It is worth noting that the above control law is a filtered version of the original PI regulator. The positive real quantity $a$ is a design parameter to be defined later.

#### 3.3.2 Outer Loop Singular Perturbation System

**Remark 4.** The outer loop model, combined with the reduced-state model (30) and the control law (34), takes the form of regularly perturbed differential equations (see Chapter 6 in [10]). In view of the fact that $\varepsilon_0 = L/R^2C$ has a small value, we can normalize $\varepsilon_0$ to $\varepsilon_2$, and so we put $L/C = \varepsilon_0 R^2 = \varepsilon_0\vartheta$ with $0 < \vartheta_{\min} \le \vartheta \le \vartheta_{\max}$.

According to the above, the closed-loop dynamics described by (30) and (34) takes the following state model:

$$\varepsilon_2\frac{dY}{dt} = g_F(X, Y, \varepsilon_2, t) \tag{35a}$$

$$\frac{dx_2}{dt} = f_{Sout}(X, Y, \varepsilon_2, t) \tag{35b}$$

where $Y = \begin{pmatrix} y_1 & y_2 \end{pmatrix}^T \overset{def}{=} \begin{pmatrix} \beta & \varepsilon_2\dot{\beta} \end{pmatrix}^T$, $g_F(X, Y, \varepsilon_2, t) = \begin{pmatrix} y_2 \\ k_2\left(\frac{e_2}{T_2} - f_{sout}(X, Y, \varepsilon_2, t)\right) - ay_2 \end{pmatrix}$, $f_{sout}(X, Y, \varepsilon_2, t) = -\frac{x_2}{RC} + \frac{E_n y_1 - r_L y_1^2 - C\vartheta y_2 y_1}{2Cx_2} - \frac{\left(E_n y_1 - r_L y_1^2 - C\vartheta y_2 y_1\right)}{2Cx_2}\cos(2\omega_n t) + \varepsilon_2\frac{\vartheta\omega_n}{2x_2}y_1^2\sin(2\omega_n t)$.

Passing to the fast time scale $\tau_2 = t/\varepsilon_2$ and moving $\varepsilon_2$ towards zero, the fast dynamic subsystem (FDS) of the outer loop is defined by:

$$\frac{dY}{d\tau_2} = g_F(X, Y, 0, t) \tag{36a}$$

$$\frac{dx_2}{d\tau_2} = 0 \tag{36b}$$

**Remark 5.** During the fast transient in (36a), $X$ is treated as the frozen parameter.

Following the fast decay of the transients in (36a), the equilibrium is obtained which entails singularities due to the presence of the periodically vanishing term $(1-\cos(2\omega_n t))$. To overcome this issue, the averaging technique is proposed to be applied to the system (35a) and (35b) which is periodic with period-$2\pi$ (see Appendix part of slow/fast analysis). Thus, the steady-state (more precisely, quasi-steady state) tends toward, in the mean, a stable equilibrium $Y_0^S$ given by:

$$Y_0^S = \begin{pmatrix} E_n \dfrac{1-\sqrt{1-\dfrac{8r_L C x_{2,0}}{E_n^2}\left(\dfrac{x_{2,0}}{RC}+\dfrac{e_{2,0}}{T_2}\right)}}{2r_L} \\ 0 \end{pmatrix} \quad (37a)$$

The above equation is valid under the following condition:

$$\frac{E_n^2}{8r_L C} > x_{2,0}\left(\frac{x_{2,0}}{RC}+\frac{e_{2,0}}{T_2}\right) \quad (37b)$$

As the FDS (36a) of the outer loop is nonlinear, its linearized version of the average Jacobian matrix defined by (37c) is examined to analyze the stability properties of FDS

$$A_{gF,0} = \begin{pmatrix} 0 & 1 \\ -\dfrac{k_2 E_n}{2Cx_{2,0}}\sqrt{1-\dfrac{8r_L C x_{2,0}}{E_n^2}\left(\dfrac{x_{2,0}}{RC}+\dfrac{e_{2,0}}{T_2}\right)} & A_{gF,0\_4} \end{pmatrix} \quad (37c)$$

with $A_{gF,0\_4} = \dfrac{k_2 \vartheta E_n}{4r_L x_{2,0}}\left(1-\sqrt{1-\dfrac{8r_L C x_{2,0}}{E_n^2}\left(\dfrac{x_{2,0}}{RC}+\dfrac{e_{2,0}}{T_2}\right)}\right)-a$.

According to (37c) and taking into account that $a > 0$, we conclude that $A_{gF,0}$ is a Hurwitz matrix if and only if the design parameter $k_2$ is positive and the following condition holds:

$$\frac{a}{k_2} > \frac{\vartheta E_n}{4r_L x_{2,0}}\left(1-\sqrt{1-\frac{8r_L C x_{2,0}}{E_n^2}\left(\frac{x_{2,0}}{RC}+\frac{e_{2,0}}{T_2}\right)}\right) \quad (37d)$$

By replacing $Y$ in (35b) with (37a), the average reduced SDS of the outer loop occurs according to

$$\dot{x}_{2,0} = \frac{e_{2,0}}{T_2} \quad (38)$$

**Proposition 3.** Consider the singular perturbation of the outer loop system described by (35a) and (35b). According to remark 5, one has:

i. The FDS (36a) is exponentially stable and $Y$ converges exponentially (in the mean) to $Y_0^S$ if the gain $k_2$ and the parameter $a$ have positive values $k_2 > 0$ and $a > 0$ such that the requirement (37d) is fulfilled.

ii. The behavior of $x_2$ is defined by the stable reference equation of the form (38). The requirement $\lim_{t\to\infty} e_2(t) = 0$ is then achieved.

## 4 Control System Analysis

The following theorem demonstrates that the control goals are achieved (in the mean) with precision depending on the network frequency $\rho = 1/\omega_n$ and the positive small parameters $\varepsilon_i$ ($i = 1, 2$).

**Theorem.** (Main result) Consider the PWM AC/DC full-bridge boost rectifier represented by its average model (3a) and (3b), and illustrated in Fig. 2 in association with the cascade controller composed of the inner controller (25) and the outer controller (34). The resulting closed-loop system presents the following properties:

1. The error $e_1 = x_1^* - x_1$ vanishes exponentially fast (where $x_1^* = \beta v_n/E_n$).
2. Let the control design parameters be chosen such that the following inequalities are respected $0 < \varepsilon_1\varepsilon_2 \ll \varepsilon_2 \ll 1$, $T_1 < T_2$, $k_1 < 0$, $k_2 < 0$, $a > 0$, and $\dfrac{a}{k_2} > \dfrac{\vartheta E_n}{4r_L x_{2,0}}\left(1-\sqrt{1-\dfrac{8r_L C x_{2,0}}{E_n^2}\left(\dfrac{x_{2,0}}{RC}+\dfrac{e_{2,0}}{T_2}\right)}\right)$. Then, there exist positive constants $\rho^*$ and $\varepsilon_i^*$ ($i = 1, 2$) such that for $0 < \rho < \rho^*$ and $0 < \varepsilon_i < \varepsilon_i^*$ ($i = 1, 2$), one gets:

The tracking errors $e_1$, $e_2$, the tuning signal $y_1$ and its derivative $y_2$, and $Z$ are harmonic signals continuously depending on $\varepsilon_i$ ($i = 1, 2$) and $\rho$, i.e. $e_1(t, \varepsilon_i, \rho)$, $e_2(t, \varepsilon_i, \rho)$, $y_1(t, \varepsilon_i, \rho)$, $y_2(t, \varepsilon_i, \rho)$, $Z(t, \varepsilon_i, \rho)$. Furthermore, one has

$$\lim_{\substack{\varepsilon_i\to 0\\ \rho\to 0}} e_1(t,\varepsilon_i,\rho) = 0, \qquad \lim_{\substack{\varepsilon_i\to 0\\ \rho\to 0}} e_2(t,\varepsilon_i,\rho) = 0,$$

$$\lim_{\substack{\varepsilon_i\to 0\\ \rho\to 0}} y_1(t,\varepsilon_i,\rho) = E_n\frac{1-\sqrt{1-\dfrac{8r_L (x_2^*)^2}{RE_n^2}}}{2r_L}, \qquad \lim_{\substack{\varepsilon_i\to 0\\ \rho\to 0}} y_2(t,\varepsilon_i,\rho) = 0,$$

$$\lim_{\substack{\varepsilon_i\to 0\\ \rho\to 0}} Z(t,\varepsilon_i,\rho) = 0.$$

**Proof of Theorem.** In order to lighten the presentation of this paper, the proof of the Theorem is placed in the appendix.

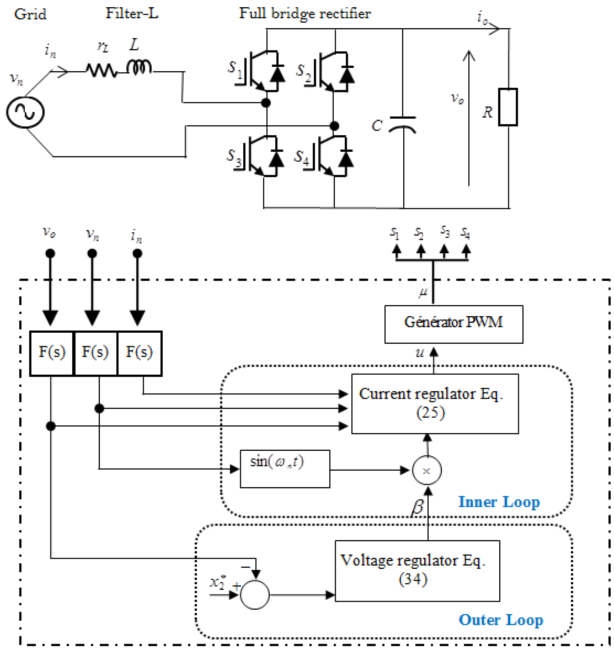


**Fig. 2** Full-bridge PWM boost rectifier with nonlinear controller.

**Remark 6.**

i. The proof of the theorem (see Appendix) provides the Lyapunov functions of the boundary layer and the reduced system for the slow/fast subsystem and for the complete slow/fast/ultra-fast system. These Lyapunov functions allow us to provide exact mathematical expressions for the upper limits of the singularly perturbed parameters $\varepsilon_1$ and $\varepsilon_2$ by constructing additional conditions [13].

ii. Part *Slow/Fast Subsystem Stability Analysis* in the theorem proof can be used to demonstrate the analytical approach used in section 3.3.2 in which the averaging technique is adopted to overcome the singularity problem.

## 5 Simulation

The experimental setup illustrated in Fig. 2, including the control laws (25), and (34) developed in Section 3, will now be tested by simulation in the MATLAB/Simulink platform using the parameter values listed in Tables 2 and 3. In fact, for the simulation process, the ODE14x (Extrapolation) solver is picked with a fixed step time of $10^{-6}$s.

### 5.1 Control Performance in Presence of Constant Load

Figs. 3 to 7 aim to illustrate the behavior of the regulators in response to the change in the output voltage reference value $x_2^*$. Specifically, the reference value changes from 600 V to 700 V and then to 500 V (see Fig. 3), while the load is kept constant at $R$ = 60 Ω.

The output voltage $v_o$ converges, in the mean, to their reference values as seen in Fig. 3, and it rapidly settles down with each variation in the reference. Besides, the voltage ripples are seen to oscillate at the frequency $2\omega_n$, but their amplitude is too small in comparison to the average magnitude of the signals (< 2% as seen in Fig. 3), confirming the Theorem. Figs. 4(a) and 4(b) show the measured input current $i_n$ response with a lower THD value equal to 1,59% (see Fig. 4(b)). In Fig. 4(a), it can be seen that the current follows its sinusoidal reference $x_1^*$ with the desired characteristics (amplitude and frequency). Fig. 5 indicates that the current frequency is fixed and equal to the voltage frequency $\omega_n$. In fact, the current stays in phase with the supply net voltage $v_n$ most of the time complying with the PFC requirement. This is illustrated further by Fig. 6 which means that, after the transient phases caused by the reference voltage steps, the ratio $\beta$ always takes a constant value. It also indicates that the ripple phenomenon has no effect on the outer-loop control signal $\beta$, confirming the separation mode between the inner and outer loops. Fig. 7 shows that the corresponding inner-loop control signal $u$ is limited to the interval [–1, 1].

**Table 2** Full bridge AC/DC boost rectifier characteristics.

| Parameters | Symbols | Values |
|---|---|---|
| Network | $E_n/f_n$ | 220√2[V]/50 [Hz] |
| L-filter | $L/r_L$ | 1 [mH]/890 [mΩ] |
| DC capacitance | $C$ | 5 [mF] |
| PWM switching frequency | $f_s = 1/T_s$ | 24 [kHz] |
| Load | $R$ | 60 [Ω] |

**Table 3** Controller parameters.

| Parameters | Symbols | Values |
|---|---|---|
| Current regulator | $\varepsilon_1$ | $2\times10^{-6}$ |
| | $T_1$ | $10^{-3}$s |
| | $k_1$ | $-2.1\times10^{-7}$ |
| Voltage regulator | $\varepsilon_2$ | $2.71\times10^{-3}$ |
| | $T_2$ | $3.71\times10^{-2}$s |
| | $k_2$ | $4.73\times10^{-3}$ |
| | $a$ | 1 |

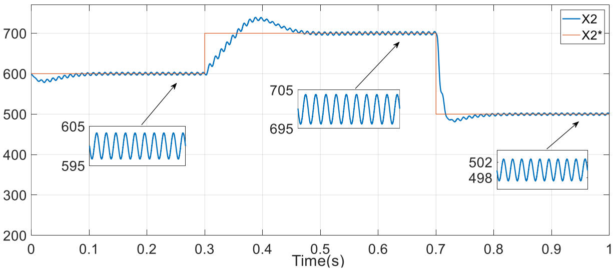


**Fig. 3** Output voltage $x_2$ in response to a step in the reference.

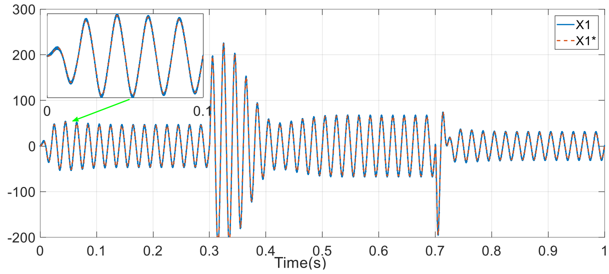


(a)

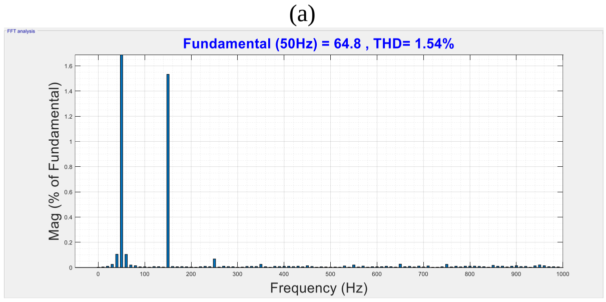


(b)

**Fig. 4** a) Input current $x_1$ and its reference $x_1^*$ and b) Harmonic content of the grid current.

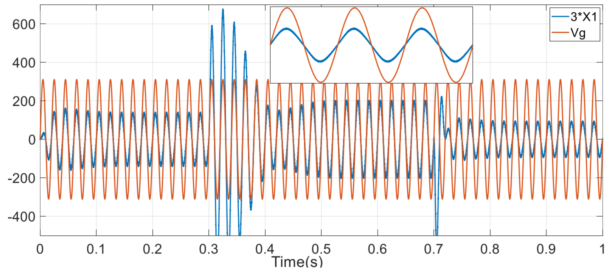


**Fig. 5** Input current $x_1$ in response to load changes: PFC checking.

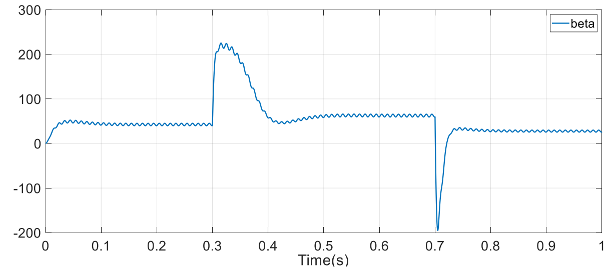


**Fig. 6** Variation of the ratio $\beta$ in response to a varying reference voltage.

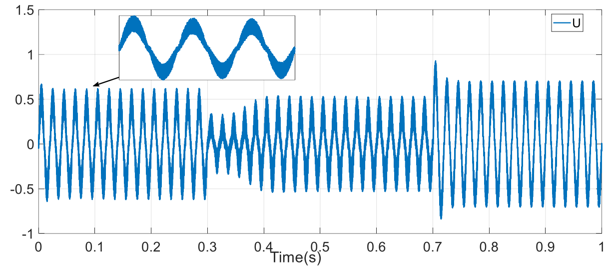


**Fig. 7** Control signal.

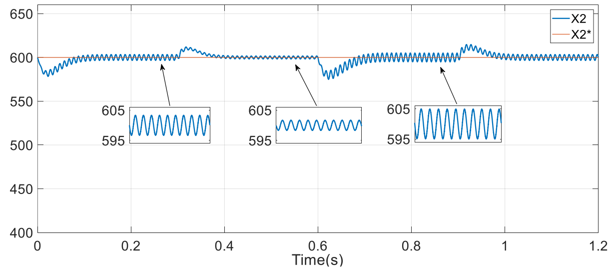


**Fig. 8** Output voltage $x_2$ in response to load changes.

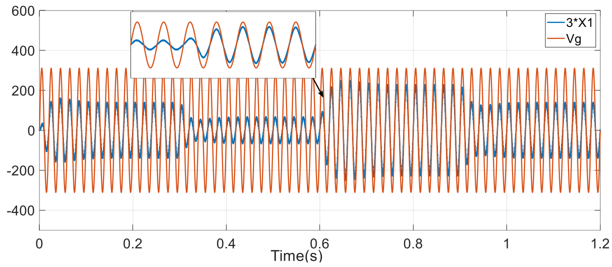


**Fig. 9** PFC in response to load changes.

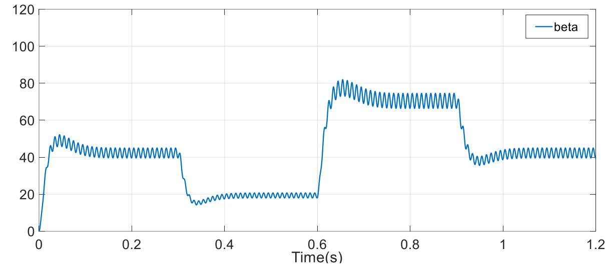


**Fig. 10** Variation of the ratio $\beta$ in response to load changes.

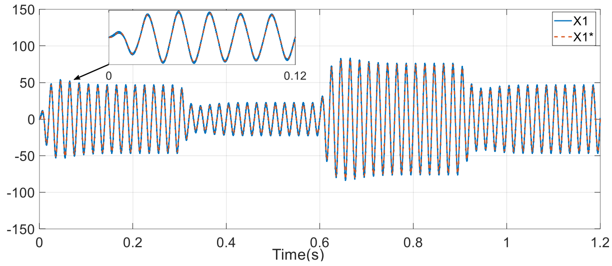


**Fig. 11** Input current $x_1$ and its reference $x_1^*$.

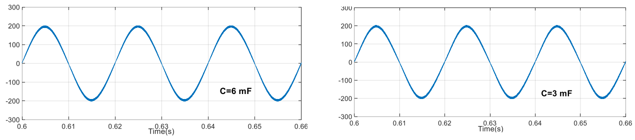


Input current $x_1$.

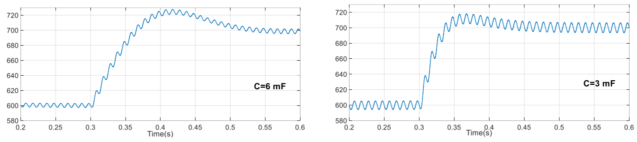


Output voltage $x_2$.

**Fig. 12** Effect of the filter capacitance.

### 5.2 Control Performance in Presence of Load Change

In order to evaluate the robustness potential of the proposed controller, a load change is operated which is not included in the controller configuration. More precisely, the load changes at 0.3s, from its nominal value (60 Ω) to the double value (120 Ω). Then, at 0.6 s, it goes from (120 Ω) to (40 Ω). Finally, the load returns to its initial value (60 Ω) at 0.9 s. Except for the load variations, all other elements of the circuit remain unchanged.

The reference of the DC output voltage is kept constant equal to 600 V. Fig. 8 shows that the disturbing influence of load variations on the output voltage $x_2$ is well corrected by the regulator. We validate that, with the variations of the load, the input current and network voltage are sinusoidal and in phase, and that the amplitude of the current varies inversely. As shown in Fig. 9, the PFC property is maintained in spite of load variations.

Furthermore, Fig. 10 shows that after the transitional (finite) periods concerning load changes, the ratio $\beta$ takes on constant values, which allows unitary power factor to be achieved. Fig. 11 shows the evolution of the input current of $x_1$, it can be seen that the current always follows its sinusoidal reference value $x_1^*$ despite the load changes.

### 5.3 Effect of the Filter Capacitance

Fig. 12 shows how the filter capacitance affects the input current and output voltage with two different capacitance values ($C$ = 6 mF and $C$ = 3 mF). Except for this change, all remaining system characteristics are kept unchanged. For both capacitances, it is clear that the two desired control objectives (power factor correction and output voltage regulation) are achieved in the mean. It is observed that the larger capacitance provides lower ripples while the smaller capacitance provides a rapid transient.

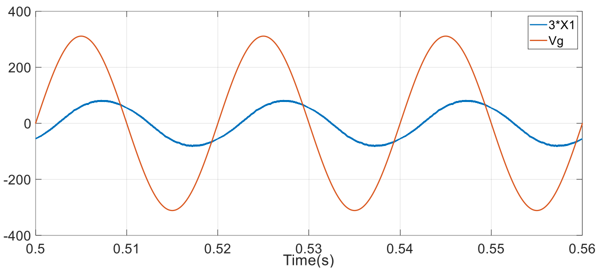


**Fig. 13** Cheeking PFC for $r_L = 0.6\ \Omega$ (no separation).

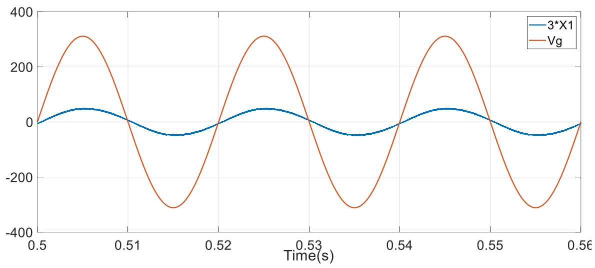


**Fig. 14** Cheeking PFC for $r_L + R_{ad} = 4\ \Omega$ (separation).

### 5.4 Time-Scale Separation Verification

In order to verify the relevance of requirement (17), simulations were performed for the open-loop AC/DC rectifier by testing two cases (Figs. 13 and 14) according to the resistance value $r_L$. In this case, a duty cycle step was applied, from 60% to 70%, and the other parameters are listed in Table 1. Fig. 12 shows that the separation requirement is not verified for $r_L = 0.6\ \Omega$, whereas this requirement is verified in Fig. 13 for $r_L = 4\ \Omega$ (practically an additional resistance $R_{ad}$ is added in series with the resistance $r_L$). Therefore, the estimated efficiency with separation is extremely satisfactory for the power factor correction requirement.

## 6 Conclusion

In the present study, we dealt with the issue of controlling a boost-type full-bridge rectifier. The PFC was examined by deriving the time-scale separation principle which can be considered as a solution for the converter optimization problem before developing an advanced control technique for PWM AC/DC converters. The time-scale separation can be accomplished by choosing the appropriate value for the circuit components (inductance, capacitance, and the parasitic resistance).

Based on the 2$^{nd}$ order nonlinear state-space averaged system (3a) and (3b), a new control strategy has been developed, using the three-time-scale singular perturbation technique, to achieve the PFC objective and the DC bus regulation. A formal stability analysis has also taken part in this study using specialized control theory methods, such as the multi-time-scale singular perturbation technique and averaging theory. The results were verified by numerical simulation tests, which further demonstrated the robustness of the controller performance vis-à-vis considerable changes in load.

## Appendix (Proof)

**Part 1:** has already been established in Proposition 1.

**Part 2:** In order to prove the second part of Theorem, let us introduce, the augmented state vectors $Z = u$, $Y = (y_1\ y_2)^T = (\beta_1\ \varepsilon\beta_1)^T$, and $X = (x_1\ x_2)^T$. Then, from (26a) and the first equation of (26b), and (35a-b) in which the derivative $\dot{x}_1^*$ can be replaced by $\dot{x}_1^* = \frac{y_2}{\varepsilon_2}\sin(\omega_n t) + \omega_n y_1 \cos(\omega_n t)$. We obtain

$$\varepsilon_1\varepsilon_2\dot{Z}(t) = h(t, X, Y, Z, \varepsilon) \quad \text{(A1a)}$$

$$\varepsilon_2\dot{Y}(t) = g(t, X, Y, \varepsilon) \quad \text{(A1b)}$$

$$\dot{X}(t) = f(t, X, Y, Z, \varepsilon) \quad \text{(A1c)}$$

where $\varepsilon = (\varepsilon_1\ \varepsilon_2)$, $h(t, X, Y, Z, \varepsilon) = k_1\left(\frac{e_1}{T_1} - f_{1.1}(X, Z) + f_{1.2}(t, Y, \varepsilon)\right)$, $g(t, X, Y, \varepsilon) = \begin{pmatrix} y_2 \\ k_2\left(\frac{e_2}{T_2} - f_{2.1}(X, Y) - f_{2.2}(t, X, Y, \varepsilon)\right) - ay_2 \end{pmatrix}$, $f(t, X, Y, Z, \varepsilon) = \begin{pmatrix} f_{1.1}(X, Z) + \frac{E_n}{L}\sin(\omega_n t) \\ f_{2.1}(X, Y) + f_{2.2}(t, X, Y, \varepsilon) \end{pmatrix}$ with $f_{1.1}(X, Z) = -\frac{x_2}{L}Z - \frac{r_L}{L}x_1$, $f_{1.2}(t, Y, \varepsilon) = \left(\frac{y_2}{\varepsilon_2} - \frac{E_n}{L}\right)\sin(\omega_n t) + \omega_n y_1\cos(\omega_n t)$, $f_{2.1}(X, Y) = -\frac{x_2}{RC} + \frac{E_n y_1 - r_L y_1^2 - C\vartheta y_2 y_1}{2Cx_2}$, $f_{2.2}(t, X, Y, \varepsilon) = -\frac{\left(E_n y_1 - r_L y_1^2 - C\vartheta L y_1 y_2\right)\cos(2\omega_n t)}{2Cx_2} + \frac{\varepsilon_2\vartheta\omega_n y_1^2\sin(2\omega_n t)}{2x_2}$.

The averaging theory (Chapter 10 in [12]), [6, 7], and then the three-time scale singular perturbation method will now be used to study the stability properties of the time-varying system (A1a)-(A1c).

Let us now introduce the time-scale change $\bar{t} = \omega_n t$ in (A1a)-(A1c). It follows that $\bar{Z}(\bar{t}) \overset{\text{def}}{=} Z(\bar{t}/\omega_n)$, $\bar{Y}(\bar{t}) \overset{\text{def}}{=} Y(\bar{t}/\omega_n)$, and $\bar{X}(\bar{t}) \overset{\text{def}}{=} X(\bar{t}/\omega_n)$ undergo the differential equations

$$\varepsilon_1\varepsilon_2\dot{\bar{Z}}(\bar{t}) = \rho\bar{h}(\bar{t}, \bar{X}, \bar{Y}, \bar{Z}, \varepsilon, \rho) \quad \text{(A2a)}$$

$$\varepsilon_1\varepsilon_2\dot{\bar{Y}}(\bar{t}) = \rho\bar{g}(\bar{t}, \bar{X}, \bar{Y}, \varepsilon, \rho) \quad \text{(A2b)}$$

$$\dot{\bar{X}}(\bar{t}) = \rho\bar{f}(\bar{t}, \bar{X}, \bar{Y}, \bar{Z}, \varepsilon, \rho) \quad \text{(A2c)}$$

where $\rho = 1/\omega_n$. In view of (A1a)-(A1c) and (A2a)-(A2c), it seems that $\bar{h}(\bar{t}, \bar{X}, \bar{Y}, \bar{Z}, \varepsilon, \rho)$, $\bar{g}(\bar{t}, \bar{X}, \bar{Y}, \varepsilon, \rho)$, and $\bar{f}(\bar{t}, \bar{X}, \bar{Y}, \bar{Z}, \varepsilon, \rho)$ as functions of $\bar{t}$ are periodic with period $2\pi$. Therefore, the averaged functions are introduced as:

$$h_0\left(X_0, Z_0\right) \overset{\text{def}}{=} \lim_{\rho \to 0} \frac{1}{2\pi} \int_0^{2\pi} \bar{h}(\bar{t}, \bar{X}, \bar{Y}, \bar{Z}, \varepsilon, \rho) d\bar{t} \tag{A3a}$$

$$g_0\left(X_0, Y_0\right) \overset{\text{def}}{=} \lim_{\rho \to 0} \frac{1}{2\pi} \int_0^{2\pi} \bar{g}(\bar{t}, \bar{X}, \bar{Y}, \varepsilon, \rho) d\bar{t} \tag{A3b}$$

$$f_0\left(X_0, Y_0, Z_0\right) \overset{\text{def}}{=} \lim_{\rho \to 0} \frac{1}{2\pi} \int_0^{2\pi} \bar{f}(\bar{t}, \bar{X}, \bar{Y}, \bar{Z}, \varepsilon, \rho) d\bar{t} \tag{A3c}$$

Given that the system under consideration has an equilibrium $Z_0^* = 0$, $Y_0^* = \left(y_{1,0}^* \quad y_{2,0}^*\right)^{\mathrm{T}} = \left(y_{1,0}^* \quad 0\right)^{\mathrm{T}}$, and $X_0^* = \left(x_{1,0}^* \quad x_2^*\right)^{\mathrm{T}} = \left(0 \quad x_2^*\right)^{\mathrm{T}}$ different from zero, we introduce the following variables changes that allow us to define the last system in terms of error dynamics: $\tilde{Z}_0 = \left(Z_0 - Z_0^*\right) = Z_0$, $\tilde{Y}_0 = \left(\tilde{y}_{1,0} \;\; \tilde{y}_{2,0}\right)^{\mathrm{T}} = \left(y_{1,0} - y_{1,0}^* \;\; y_{2,0}\right)^{\mathrm{T}}$, $\tilde{X}_0 = \left(\tilde{x}_{1,0} \;\; \tilde{x}_{2,0}\right) = \left(x_{1,0} \;\; x_{2,0} - x_2^*\right)$. Starting from (A1a)-(A1c) and according to (A3a)-(A3c), the closed-loop error dynamics are reformulated as follows:

$$\varepsilon_1 \varepsilon_2 \dot{\tilde{Z}}_0(\bar{t}) = \rho \hat{h}_0(\tilde{X}_0, \tilde{Z}_0) = \rho k_1 \left( -\frac{\tilde{x}_{1,0}}{T_1} - \tilde{f}_{1.1,0} \right) \tag{A4a}$$

$$\varepsilon_2 \dot{\tilde{Y}}_0(\bar{t}) = \rho \hat{g}_0(\tilde{X}_0, \tilde{Y}_0) = \rho \begin{pmatrix} \tilde{y}_{2,0} \\ k_2\left( -\frac{\tilde{x}_{2,0}}{T_2} - \tilde{f}_{2.1,0} \right) - a\tilde{y}_{2,0} \end{pmatrix} \tag{A4b}$$

$$\dot{\tilde{X}}_0(\bar{t}) = \rho \tilde{f}_0(\tilde{X}_0, \tilde{Y}_0, \tilde{Z}_0) = \rho \begin{pmatrix} \tilde{f}_{1.1,0} \\ \tilde{f}_{2.1,0} \end{pmatrix} \tag{A4c}$$

where $\tilde{f}_{1.1,0}(\tilde{X}_0, \tilde{Z}_0) = -\frac{\left(\tilde{x}_{2,0} + x_2^*\right)}{L} \tilde{Z}_0 - \frac{r_L}{L} \tilde{x}_{1,0}$, $\tilde{f}_{2.1,0}(\tilde{X}_0, \tilde{Y}_0) = -\frac{\left(\tilde{x}_{2,0} + x_2^*\right)}{RC} + \frac{E_n\left(\tilde{y}_{1,0} + y_{1,0}^*\right)}{2C\left(\tilde{x}_{2,0} + x_2^*\right)} - \frac{r_L\left(\tilde{y}_{1,0} + y_{1,0}^*\right)^2}{2C\left(\tilde{x}_{2,0} + x_2^*\right)} - \frac{\vartheta\left(\tilde{y}_{1,0} + y_{1,0}^*\right)\tilde{y}_{2,0}}{2\left(\tilde{x}_{2,0} + x_2^*\right)}$.

For the average system (A4a)-(A4c), the stability analysis is inspired by the three-time-scale technique discussed in [15], which is based on the assumption that for $0 < \varepsilon_1\varepsilon_2 \ll \varepsilon_2 < 1$, the dynamics of $\tilde{X}_0$, $\tilde{Y}_0$, and $\tilde{Z}_0$ can be approximated by three models: the SDS, FDS, and UFDS. It is important to ensure that the trajectory of the UFDS (A4a) does not shift from the following quasi-steady-state equilibrium.

$$\tilde{Z}_0 = \tilde{h}_0(\tilde{X}_0) = -\frac{L}{\left(\tilde{x}_{2,0} + x_2^*\right)} \left( \frac{r_L}{L}\tilde{x}_{1,0} - \frac{\tilde{x}_{1,0}}{T_1} \right) \tag{A5a}$$

Hence, the UFDS (A4a) according to $\hat{Z}_0 = \tilde{Z}_0 - \tilde{h}_0\left(\tilde{X}_0\right)$ is defined, for the stretched time-scale $\tau_{1,0} = \bar{t} / \varepsilon_1\varepsilon_2$, as follows

$$\frac{d\hat{Z}_0}{d\tau_{1,0}} = \rho \hat{h}_0(\tilde{X}_0, \hat{Z}_0 + \tilde{h}_0(\tilde{X}_0)) = \rho k_1 \frac{\left(\tilde{x}_{2,0} + x_2^*\right)}{L} \hat{Z}_0 \tag{A5b}$$

Similar to the UFDS, it is also necessary to ensure that the FDS (A4b) does not shift from the following equilibrium

$$\tilde{Y}_0 = \tilde{g}_0(\tilde{X}_0) = \begin{pmatrix} E_n \frac{1-\psi_1}{2r_L} - y_{1,0}^* \\ 0 \end{pmatrix} \tag{A6a}$$

where $\psi_1 = \sqrt{1 - \frac{8r_L C\left(\tilde{x}_{2,0} + x_2^*\right)}{E_n^2} \left( \frac{\left(\tilde{x}_{2,0} + x_2^*\right)}{RC} - \frac{\tilde{x}_{2,0}}{T_2} \right)}$. So, the FDS with regard to $\hat{Y}_0 = \tilde{Y}_0 - \tilde{g}_0\left(\tilde{X}_0\right)$ is defined, for the stretched time-scale $\tau_{2,0} = \bar{t} / \varepsilon_2$, as follows

$$\frac{d\hat{Y}_0}{d\tau_{2,0}} = \rho \hat{g}_0(\tilde{X}_0, \hat{Y}_0 + \tilde{g}_0(\tilde{X}_0)) = \rho \begin{pmatrix} \hat{y}_{2,0} \\ \Psi \end{pmatrix} \tag{A6b}$$

where $\Psi(\tilde{X}_0, \hat{Y}_0 + \tilde{g}_0(\tilde{X}_0)) = -\frac{k_2 E_n \psi_1}{2C\left(\tilde{x}_{2,0} + x_2^*\right)} \hat{y}_{1,0} + \frac{k_2 r_L}{2C\left(\tilde{x}_{2,0} + x_2^*\right)} \hat{y}_{1,0}^2 + \psi_2 \hat{y}_{2,0} + \frac{k_2 \vartheta}{2\left(\tilde{x}_{2,0} + x_2^*\right)} \hat{y}_{1,0}\hat{y}_{2,0}$ and $\psi_2 = \frac{k_2\vartheta\left(E_n - E_n\psi_1\right)}{4r_L\left(\tilde{x}_{2,0} + x_2^*\right)} - a$.

Finally, the SDS subsystem is obtained by substituting the UFDS equilibrium $\tilde{Z}_0 = \tilde{h}_0\left(\tilde{X}_0\right)$ and the FDS equilibrium $\tilde{Y}_0 = \tilde{g}_0\left(\tilde{X}_0\right)$ given, successfully, by (A5a) and (A6a) into (A4c). One gets

$$\dot{\tilde{X}}_0 = \rho \tilde{f}_0(\tilde{X}_0, \tilde{g}_0(\tilde{X}_0), \tilde{h}_0(\tilde{X}_0)) = \rho \begin{pmatrix} -\tilde{x}_{1,0}/T_1 \\ -\tilde{x}_{2,0}/T_2 \end{pmatrix} \tag{A7b}$$

The obtained subsystems (A5b), (A6b), and (A7a) can now be used in a sequential (double) time-scale analysis (Chapter 11 in [12]) to demonstrate, in the first step, the stability properties of the degenerate subsystem designated as *slow/fast*, and then, in the second step, the stability properties of the complete system designated as slow-fast/ultra-fast.

**Slow/Fast Subsystem (SF) Stability Analysis:**

At this stage, we consider the Slow/Fast subsystem, consisting of (A4b) and (A4c) in which $\tilde{Z}_0$ is replaced by its quasi-steady-state equilibrium (A5a). One obtains

$$\varepsilon_2 \dot{\tilde{Y}}_0(\bar{t}) = \rho \hat{g}_0(\tilde{X}_0, \tilde{Y}_0) \tag{A8a}$$

$$\dot{\tilde{X}}_0(\bar{t}) = \rho \tilde{f}_0(\tilde{X}_0, \tilde{Y}_0, \tilde{h}_0(\tilde{X}_0)) \tag{A8b}$$

The stability of the origin $(\tilde{X}_0 = 0, \tilde{Y}_0 = 0)$ can be guaranteed by meeting certain requirements for all $\tilde{X}_0 \in \Omega_{\tilde{X}_0}$ and $\hat{Y}_0 \in \Omega_{\hat{Y}_0}$.

- The origin $(\tilde{X}_0 = 0, \tilde{Y}_0 = 0)$ is an isolated equilibrium of (A8a) and (A8b) where

$0=\tilde{f}_0(0,0,\tilde{h}_0(\tilde{X}_0,\tilde{Y}_0))$ and $0=\hat{g}_0(0,0)$. Moreover, $\tilde{Y}_0=\tilde{g}_0(\tilde{X}_0)$ is the root of $0=\hat{g}_0(\tilde{X}_0,\tilde{Y}_0)$ which vanishes at $\tilde{X}_0=0$, and $\|\tilde{g}_0(\tilde{X}_0)\|\le\Theta_1(\|(\tilde{X}_0)\|)$ with $\Theta_1(.)$ is a $\kappa$ function.

- The functions $\hat{g}_0(\tilde{X}_0,\tilde{Y}_0)$, $\tilde{f}_0(\tilde{X}_0,\tilde{Y}_0,\tilde{h}_0(\tilde{X}_0))$, and $\tilde{g}_0(\tilde{X}_0)$, are continuously differentiable and bounded for $\hat{Y}_0\in\Omega_{\hat{Y}_0}$.
- The origin of the reduced system (A7a) is exponentially stable. Additionally, its associated Lyapunov function is defined by

$$V_S(\tilde{X}_0)=\frac{1}{2\rho}\left(T_1q_{S1}x_{1,0}^2+T_2q_{S2}x_{2,0}^2\right) \tag{A8c}$$

where $q_{S1}$ and $q_{S2}$ are positive constants.

- According to the proposition (3–Part 1), it is shown that the boundary layer (A6b) is exponentially stable for positive values of $k_2$ and $a$ such that

$$\frac{a}{k_2}>\frac{\vartheta\left(E_n-E_n\psi_1\right)}{4r_L\left(\tilde{x}_{2,0}+x_2^*\right)} \tag{A8d}$$

Furthermore, using the Lyapunov indirect method, the associated Lyapunov function is defined by

$$V_F(\tilde{X}_0,\hat{Y}_0)=\frac{1}{2\rho}\left(p_{F1}\hat{y}_{1,0}^2+p_{F2}\hat{y}_{2,0}^2+2p_{F3}\hat{y}_{1,0}\hat{y}_{2,0}\right) \tag{A8e}$$

and their solutions are given by

$$p_{F1}=-\left(\frac{C\left(\tilde{x}_{2,0}+x_2^*\right)\psi_2}{2k_2\psi_1}+\frac{1}{2\psi_2}\right)q_{F1}-\frac{k_2\psi_1}{2C\left(\tilde{x}_{2,0}+x_2^*\right)\psi_2}q_{F2} \tag{A8f}$$

$$p_{F2}=\frac{1}{\psi_2}\left(-\frac{C\left(\tilde{x}_{2,0}+x_2^*\right)}{2k_2\psi_1}q_{F1}-\frac{q_{F2}}{2}\right) \tag{A8g}$$

$$p_{F3}=\frac{C\left(\tilde{x}_{2,0}+x_2^*\right)}{2k_2\psi_1}q_{F1} \tag{A8h}$$

in which $\tilde{X}_0$ is treated as a fixed parameter. $q_{F1}$ and $q_{F2}$ are positive constants.

Therefore, from the singular perturbation theory (Theorem 11.4 in [12]), it follows that there exists $\varepsilon_2^*>0$ such that for all $\varepsilon_2>\varepsilon_2^*$ the origin $(\tilde{X}_0=0,\ \tilde{Y}_0=0)$ of (A8a) and (A8b) is exponentially stable. Moreover, for the *Slow*/*Fast* **s**ubsystem, a new Lyapunov function candidate $V_{SF}(\tilde{X}_0,\hat{Y}_0)$ is considered for all $0<\eta<1$

$$V_{SF}(\tilde{X}_0,\hat{Y}_0)=(1-\eta_2)V_S(\tilde{X}_0)+\eta_2V_F(\tilde{X}_0,\hat{Y}_0) \tag{A9}$$

For all $\varepsilon_2<\varepsilon_2^{\eta 2}$ where $\varepsilon_2^{\eta 2}<\varepsilon_2^*$.

**Slow-Fast/Ultra-Fast (SFU) Stability Analysis:**

Using the results obtained in the first stage, we will study the stability properties of the complete system (A4a)-(A4c), which is considered as a new two-time scale singular perturbation problem.

$$\varepsilon_1\varepsilon_2\dot{\hat{Z}}_0=\rho\hat{h}_0(\tilde{\chi}_0,\tilde{Z}_0) \tag{A10a}$$

$$\dot{\tilde{\chi}}_0=\rho\tilde{F}_0(\tilde{\chi}_0,\tilde{Z}_0) \tag{A10b}$$

where $\tilde{\chi}_0\overset{\text{def}}{=}(\tilde{Y}_0\quad\tilde{X}_0)=\left(\tilde{y}_{1,0}\quad\tilde{y}_{2,0}\quad\tilde{x}_{1,0}\quad\tilde{x}_{2,0}\right)^T$. The stability of (A10a,b) can be ensured by meeting certain requirements for all $\tilde{\chi}_0\in\Omega_{\tilde{\chi}_0}$.

- The origin $(\tilde{\chi}_0=0,\tilde{Z}_0=0)$ is an isolated equilibrium of (A10a) and (A10b) where $0=\hat{h}_0(0,0)$ and $0=\tilde{F}_0(0,0)$. In addition, $\tilde{Z}_0=\tilde{h}_0(\tilde{\chi}_0)$ is the unique root of $0=\hat{h}_0(\tilde{\chi}_0,\tilde{Z}_0)$, which vanishes at $\tilde{\chi}_0=0$, and $\|\tilde{h}_0(\tilde{\chi}_0)\|\le\Theta_2(\|(\tilde{\chi}_0)\|)$ with $\Theta_2(.)$ is a $\kappa$ function.
- The functions $\hat{h}_0$, $\tilde{F}_0$, and $\tilde{h}_0$ are continuously differentiable and bounded for $\hat{Z}_0\in\Omega_{\hat{Z}_0}$.
- The final results obtained in the first stage (for Slow/Fast subsystem) prove that the origin of the reduced system defined by $\dot{\tilde{\chi}}_0=\rho\tilde{F}_0\left(\tilde{\chi}_0,\tilde{h}_0(\tilde{\chi}_0)\right)$ is exponentially stable for $\varepsilon_2<\varepsilon_2^*$. Moreover, its associated Lyapunov function is defined by (A9).
- The origin of the boundary layer (A5b) is exponentially stable. Plus, its associated Lyapunov function is readily defined by

$$V_U\left(\tilde{\chi}_0,\tilde{Z}_0\right)=\frac{L}{2\rho k_1\left(\tilde{x}_{2,0}+x_{2,0}^*\right)}q_U\hat{Z}_0^2 \tag{A11}$$

where $\tilde{\chi}_0$ is treated as a fixed parameter and $q_U$ is a positive parameter.

Therefore, from the singular perturbation theory (e.g. Theorem 11.4 in [12, 15]), it follows that there exists $\varepsilon_1^*>0$ such that for all $\varepsilon_1<\varepsilon_1^*$ the origin of the average three-time-scale system (A4a)-(A4c) is exponentially stable. Moreover, a new Lyapunov function candidate $V_{SFU}(\tilde{\chi}_0,\hat{Z}_0)$ is considered for all $0<\eta_1<1$

$$V_{SFU}(\tilde{\chi}_0,\hat{Z}_0)=(1-\eta_1)V_{SF}(\tilde{\chi}_0)+\eta_1V_U(\tilde{\chi}_0,\tilde{Z}_0) \tag{A12}$$

for all $\varepsilon_1\varepsilon_2<\varepsilon_1^{\eta 1}\varepsilon_2^{\eta 2}$ where $\varepsilon_1^{\eta 1}<\varepsilon_1^*$.

Therefore, it can be concluded that the equilibrium $X_0^*=\left(x_{1,0}^*\quad x_{2,0}^*\right)^{\mathrm{T}}$, $Y_0^*=\tilde{g}_0(\tilde{X}_0^*)=\left(y_{1,0}^*\quad y_{2,0}^*\right)^{\mathrm{T}}$, and $Z_0^*=\tilde{h}_0(\tilde{X}_0^*)$ of the complete system is exponentially stable. Finally, Part 2 is directly concluded from the average theory (e.g.

Theorem 10.4 in [12]). The proof of the Theorem is completed.

**Intellectual Property**

The authors confirm that they have given due consideration to the protection of intellectual property associated with this work and that there are no impediments to publication, including the timing of publication, with respect to intellectual property.

**Funding**

No funding was received for this work.

**CRediT Authorship Contribution Statement**

**Y. Mchaouar:** Conceptualization, Methodology, Software, Formal analysis, Writing - Original draft. **A. Abouloifa:** Supervision. **I. Lachkar:** Data Curation. **H. Katir:** Investigation. **F. Giri:** Writing - Review and editing. **A. El Aroudi:** Validation. **A. Elallali:** Software. **C. Taghzaoui**: Investigation.

**Declaration of Competing Interest**

The authors hereby confirm that the submitted manuscript is an original work and has not been published so far, is not under consideration for publication by any other journal and will not be submitted to any other journal until the decision will be made by this journal. All authors have approved the manuscript and agree with its submission to "Iranian Journal of Electrical and Electronic Engineering".

**References**

[1] Y. Yang and K. Zhou, "Chapter 4 - Modeling and control of single-phase AC/DC converters," in *Control of power electronic converters and systems*, F. Blaabjerg, Ed. Academic Press, pp. 93–115, 2018.

[2] G. Escobar, D. Chevreau, R. Ortega, and E. Mendes, "An adaptive passivity-based controller for a unity power factor rectifier", *IEEE Transactions on Control Systems Technology*, Vol. 9, No. 4, p. 637–644, 2001.

[3] H. C. Chen and J. Y. Liao, "Bidirectional current sensorless control for the full-bridge AC/DC converter with considering both inductor resistance and conduction voltages," *IEEE Transactions on Power Electronics*, Vol. 29, No. 4, pp. 2071–2082, 2014.

[4] Y. Mchaouar, A. Abouloifa, I. Lachkar, and M. Fettach, "Analysis of the single phase full bridge bidirectional boost rectifier via singular perturbation approach with power factor correction," in *International Conference on Electrical and Information Technologies (ICEIT)*, pp. 281–287, 2016.

[5] Y. Mchaouar, A. Abouloifa, I. Lachkar, and M. Fettach, "Digital controller design for full-bridge boost rectifier using singular perturbation method based on pseudo continuous approach with power factor correction," in *International Conference on Electrical and Information Technologies (ICEIT)*, pp. 142–147, 2016.

[6] A. Abouloifa, F. Giri, I. Lachkar, and F. Z. Chaoui, "Nonlinear control design and averaging analysis of full-bridge boost rectifier," in *IEEE International Symposium on Industrial Electronics*, pp. 93–98, 2008.

[7] F. Giri, A. Abouloifa, I. Lachkar, and F. Z. Chaoui, "Formal framework for nonlinear control of PWM AC/DC boost rectifiers—Controller design and average performance analysis," *IEEE Transactions on Control Systems Technology*, Vol. 18, No 2, pp. 323–335, 2010.

[8] S. K. Kim, "Self-tuning adaptive feedback linearizing output voltage control for AC/DC converter," *Control Engineering Practice*, Vol. 45, pp. 1-11, 2015.

[9] R. Z. Scapini, L. V. Bellinaso, and L. Michels, "Stability analysis of AC–DC full-bridge converters with reduced DC-link capacitance," *IEEE Transactions on Power Electronics*, Vol. 33, No 1, pp. 899–908, 2018.

[10] V. D. Yurkevich, *Design of nonlinear control systems with the highest derivative in feedback*. World Scientific, 2004.

[11] Y. Mchaouar, C. Taghzaoui, A. Abouloifa, M. Fettach, A. Ellali, I. Lachkar, F. Giri, "Sensorless nonlinear control strategy of the single phase active power filters via two-time scale singular perturbation technique," *Universal Journal of Electrical and Electronic Engineering*, Vol. 6, No. 5, pp. 383–401, 2019.

[12] H. K. Khalil, *Nonlinear systems*. Prentice-Hall, 2002.

[13] P. Kokotovic, H. Khalil, and J. O'Reilly, *Singular perturbation methods in control: Analysis and design*. Society for Industrial and Applied Mathematics, 1999.

[14] A. Abouloifa, F. Giri, I. Lachkar, F. Z. Chaoui, M. Kissaoui, and Y. Abouelmahjoub, "Cascade nonlinear control of shunt active power filters with average performance analysis," *Control Engineering Practice*, Vol. 26, p. 211–221, 2014.

[15] S. Esteban, F. Gordillo, and J. Aracil, “Three-time scale singular perturbation control and stability analysis for an autonomous helicopter on a platform,” *International Journal of Robust and Nonlinear Control*, Vol. 23, No 12, pp. 1360–1392, 2013.

[16] V. A. Caliskan, O. C. Verghese, and A. M. Stankovic, “Multifrequency averaging of DC/DC converters,” *IEEE Transactions on Power Electronics*, Vol. 14, No 1, p. 124–133, 1999.

[17] P. T. Krein, J. Bentsman, R. M. Bass, and B. L. Lesieutre, “On the use of averaging for the analysis of power electronic systems,” *IEEE Transactions on Power Electronics*, Vol. 5, No 2, pp. 182–190, 1990.

[18] S. R. Sanders, J. M. Noworolski, X. Z. Liu, and G. C. Verghese, “Generalized averaging method for power conversion circuits,” *IEEE Transactions on Power Electronics*, Vol. 6, No. 2, pp. 251–259, 1991.

[19] J. W. Kimball and P. T. Krein, “Singular perturbation theory for DC-DC converters and application to PFC converters,” *IEEE Transactions on Power Electronics*, Vol. 23, No. 6, pp. 2970–2981, 2008.

[20] J. J. E. Slotine, J. J. E. Slotine, and W. Li, *Applied nonlinear control*. Prentice-Hall, 1991.

**Y. Mchaouar** received his degree in Electronic Engineering from Ibn Tofail University, Kenitra, Morocco. Currently, he is preparing for his Ph.D. in Electronic and Electrical Engineering, Automatic Control, and Renewable Energies at Hassan II University of Casablanca, Morocco. His research interests include observation and nonlinear control, renewable energies, active filters, AC-DC converters, and power factor correction. He has co-authored several papers on these topics.

**A. Abouloifa** received the Aggregation of Electrical Engineering from Normal High School, Rabat, Morocco, in 1999, and Ph.D. degree in Control Engineering from the University of Caen Basse-Normandie, Caen, France in 2008. He is currently a Professor at Hassan II University of Casablanca-Morocco. His main research areas include modeling, nonlinear control, and observation of FACTS systems, actives filters, uninterruptible power supplies, photovoltaic systems and multicellular converters, with power factor correction techniques. He has co-authored several papers on these topics.

**L. Lachkar** received the graduate degree from the Normal High School of Technical Education, Rabat, Morocco, in 1995 and here degree of high depth studies from the Mohammedia School of Engineers, Rabat, in 2005. She received her Ph.D. from Mohammedia School of Engineers. Currently, she is an Assistant Professor at the National School of Electricity and Mechanic. Her research interests include high-frequency power factor correction techniques, power supplies, renewable energy, active filters, and nonlinear control.

**H. Katir** received her master’s degree in Information Processing from the Faculty of Sciences Ben M’sick, Hassan II University of Casablanca, Morocco, in 2017. Currently, she is preparing her Ph.D. in the field of Automatic Control and Power Converters at Hassan II University of Casablanca, Morocco. Her research interests include nonlinear control, adaptive control, cascaded H-bridge multilevel DC/AC converters, grid-connected systems, uninterruptable power supplies, and renewable energies.

**F. Giri** has received the Ph.D. degree in Automatic Control from the Institute National Polytechnique de Grenoble, France, in 1988. He has spent long-term visits at the Laboratoire d’Automatique de Grenoble, and the University of Southern California, and Los Angeles. Since 1982, he has been successively Assistant Professor and Professor with the Mohammadia School of Engineers, Rabat-Morocco. He is currently a Professor at the University of Caen Basse-Normandie, France. His research interests include nonlinear system identification, nonlinear control, adaptive control, constrained control, power and energy systems control. He has published over 300 journal/conference papers on these topics and coauthored/coedited the books.

**A. El Aroudi** (M’00, SM’13) received the graduate degree in physical science from Faculté des Sciences, Université Abdelmalek Essaadi, Tetouan, Morocco, in 1995, and the Ph.D. degree (Hons) in applied physical science from Universitat Politècnica de Catalunya, Barcelona, Spain in 2000. During the period 1999-2001 he was a Visiting Professor at the Department of Electronics, Electrical Engineering and Automatic Control, Technical School of Engineering at Universitat Rovira i Virgili (URV), Tarragona, Spain, where he became an Associate Professor in 2001 and a full-time tenure Associate Professor in 2005. His research interests are in the field of structure and control of power conditioning systems for autonomous systems, power factor correction, renewable energy applications, stability problems, nonlinear phenomena, bifurcations control.

**A. Elallali** received her master's degree in data processing from the Faculty of Sciences Ben M'sick, Hassan II University of Casablanca, Morocco, in 2015. Currently, she is preparing for her Ph.D. in Control Systems Engineering, Electronic Engineering, Electrical Engineering and Automatic Control at Hassan II University of Casablanca, Morocco. Her research interests include nonlinear control, multilevel DC/AC converters, grid-connected systems, and renewable energies.

**C. Taghzaoui** received her master's degree in data processing from the Faculty of Sciences Ben M'sick, Hassan II University of Casablanca, Morocco, in 2015. Currently, she is preparing for her Ph.D. in the field of automatic, renewable energy, multilevel power electronics at Hassan II University, Casablanca, Morocco. The main topics of her research include simulation, modeling, non-linear control, and observation of multilevel converters.